Langmuir
Article
pubs.acs.org/Langmuir

Superhydrophobic Surfaces by Anomalous Fluoroalkylsilane Self-Assembly on Silica Nanosphere Arrays

Muhammad Akram Raza, E. Stefan Kooij,* Arend van Silfhout, and Bene Poelsema

Solid State Physics, IMPACT Institute, University of Twente, P.O. Box 217, 7500AE, Enschede, The Netherlands

Received May 10, 2010. Revised Manuscript Received June 23, 2010

We present the self-assembled formation of nanosized PFDTS (1*H*,1*H*,2*H*,2*H*-perfluorodecyltrichlorosilane) features on multilayered silica sphere arrays. We reveal the importance of residual water within the microsphere multilayers during PFDTS deposition and discuss a possible mechanism for the formation of the siloxane nanostructures. The multiscaled roughness induced by these superstructures is shown to lead to superhydrophobic behavior. The role of PFDTS is twofold: it (i) lowers the surface energy and (ii) provides the essential roughness to achieve superhydrophobicity. Moreover, the absence of PFDTS nanostructures on monolayers or in the absence of water leads to considerably smaller contact angles thereby indicating the relevance of multiscaled roughness for superhydrophobicity.

Introduction

The natural phenomenon of surface (de)wetting is a topic of high interest not only within the fundamental science community, but also for its practical application in areas such as coatings, paints, adhesives, textiles, lubrication, self-cleaning, micro/nanofluidic technology, and microelectronics.[1] More specifically, superhydrophobicity (characterized by macroscopic contact angles typically larger than 150°, combined with very small sliding angles and negligible hysteresis between advancing and receding contact angles) has attracted very substantial attention owing to its strong potential for modern technology.

The concept of artificial nonwetting surfaces was introduced by Cassie[2] six decades ago, but the real boost in this direction during the past few decades was triggered by the microscopic examination of naturally occurring superhydrophobic surfaces such as that of the lotus leaf.[3] This study revealed that the surface of the lotus leaf consists of a hierarchical roughness induced by papillae hills typically 10 μm in size, which are decorated by 100-nm-sized hair-like wax structures. Although the contact angle (CA) of sessile drops of aqueous liquids on flat wax surfaces amounts to approximately 110°, the macroscopic CA observed on the actual lotus leaf surface is more than 160° combined with very small sliding angle. It is nowadays well-established that the remarkable self-cleaning properties of these surfaces originated from the chemical nature combined with the intricate multilength scale roughness.[4]

The aforementioned revelation has proven to be a key milestone in the fabrication of artificial superhydrophobic surfaces with multiscaled roughness. Although in some attempts[5] superhydrophobicity of the surfaces was achieved with single-length scale features (nano- or micrometer-sized), only hierarchical structured roughness guarantees[6] the stability of superhydrophobicity in severe and harsh environments as exhibited by naturally occurring superhydrophobic surfaces. Different methods and techniques have been used to manufacture substrates with multiscaled/hierarchical roughness for superhydrophobic surfaces, including, for example, Langmuir−Blodgett deposition,[7] layer-by-layer deposition,[8] binary colloidal assemblies,[9] sol−gel processing,[10] laser or plasma etching,[11] and complex coating of silica nanoparticles onto cotton textiles.[12] Overall, using such methods typically involves initial generation of the multiscaled roughness structure, followed by applying a hydrophobic coating to lower its surface energy.

As mentioned, it is well-accepted that the wettability of structured surfaces is governed by two key factors: (i) surface roughness and (ii) interface chemistry. The chemical nature of the surface, combined with the liquid surface tension, determines the CA of the liquid on a perfectly clean, flat interface. Changing the surface chemistry effectively modifies the surface energy: a lower surface energy gives rise to reduced wettability and thus larger CAs.

To fabricate surfaces with low wettability, often the use of (hydrophobic) polymers with specific low surface tension endgroups is preferred. The surface tension of typical substituent endgroups decreases in the following order: CH_2 (36 dyn/cm) > CH_3 (30 dyn/cm) > CF_2 (23 dyn/cm) > CF_3 (15 dyn/cm).[13] This

*Corresponding author. e.s.kooij@tnw.utwente.nl.

(1) de Gennes, P. G.; Brochard-Wyart, F.; Quéré, D. *Capillarity and Wetting phenomena: Drops, Bubbles, Pearls, Waves*; Springer-Verlag: New York, 2004.
(2) Cassie, A. B. D.; Baxter, S. *Nature* (*London*) **1945**, *155*, 21.
(3) Barthlott, W.; Neinhuis, C. *Planta* **1997**, *202*, 1.
(4) (a) Sun, T. L.; Feng, L.; Gao, X. F.; Jiang, L. *Acc. Chem. Res.* **2005**, *38*, 644. (b) Sun, M. H.; Luo, C. X.; Xu, L. P.; Ji, H.; Qi, O. Y.; Yu, D. P.; Chen, Y. *Langmuir* **2005**, *21*, 8978.
(5) (a) Hosono, E.; Fujihara, S.; Honma, I.; Zhou, H. *J. Am. Chem. Soc.* **2005**, *127*, 13458. (b) Wier, K. A.; McCarthy, T. J. *Langmuir* **2006**, *22*, 2433.
(6) (a) Su, Y.; Ji, B.; Zhang, K; Gao, H.; Huang, Y.; Hwang, K. *Langmuir* **2010**, *26*, 4984. (b) Nosonovsky, M. *Langmuir* **2007**, *23*, 3157.
(7) Tsai, P. S.; Yang, Y. M.; Lee, Y. L. *Nanotechnology* **2007**, *18*, 465604.
(8) (a) Zhao, Y.; Li, M.; Qu, M.; Shi, Z. *Langmuir* **2008**, *24*, 12651. (b) Amigoni, S.; de Givenchy, E. T.; Dufay, M.; Guittard, F. *Langmuir* **2009**, *25*, 1073. (c) Zhai, L.; Cebeci, F. C.; Cohen, R. E.; Rubner, M. F. *Nano Lett.* **2004**, *4*, 1349.
(9) Zhang, G.; Wang, D.; Gu, Z. Z.; Mohwald, H. *Langmuir* **2005**, *21*, 9143.
(10) (a) Yeh, K. Y.; Cho, K. H.; Chen, L. J. *Langmuir* **2009**, *25*, 14187. (b) Manca, M.; Cannavale, A.; De Marco, L.; Arico, A. S.; Cingolani, R.; Gigli, G. *Langmuir* **2009**, *25*, 6357.
(11) (a) Song, X; Zhai, J.; Wang, Y.; Jiang, L. *J. Phys. Chem. B.* **2005**, *109*, 4048. (b) Teshima, K.; Sugimura, H.; Inoue, Y.; Takai, O.; Takano, A. *Appl. Surf. Sci.* **2005**, *244*, 619.
(12) (a) Leng, B.; Shao, Z.; de With, G; Ming, W. *Langmuir* **2009**, *25*, 2456. (b) Hoefnagels, H. F.; Wu, D.; de With, G; Ming, W. *Langmuir* **2007**, *23*, 13158. (c) Xue, C. H.; Jia, S. T.; Zhang, J.; Tian, L. Q. *Thin Solid Films* **2009**, *517*, 4593. (d) Xue, C. H.; Jia, S. T.; Zhang, J.; Tian, L. Q.; Chen, H. Z.; Wang, M. *Sci. Technol. Adv. Mater.* **2008**, *9*, 035008.
(13) Wang, J.; Ober, C. K. *Macromolecules* **1997**, *30*, 7560.

explains why, among the numerous molecular structures, fluorinated polymers/fluoroalkylsilanes with CF_3 endgroups are widely used as dewetting/antisticking coating.

In many studies, 1*H*,1*H*,2*H*,2*H*-perfluorodecyltrichlorosilane (PFDTS) is employed to modify the interaction between the substrate and the liquid deposited onto it. For example, Srinivasan et al.[14] used a PFDTS self-assembled monolayer (SAM) to reduce the adhesion in micro-electromechanical systems (MEMS). To prevent bulk polymerization of the highly water-sensitive trichlorosilane headgroups, the coatings were deposited under nearly water-free nitrogen-flushed conditions. Similarly, Breisch et al.[15] applied PFDTS to control the wetting behavior of fluidic microsystems.

Also on structured surfaces, PFDTS is often used to control the surface chemistry. Ogawa et al.[16] achieved ultrahydrophobicity by coating submicrometer-level roughened transparent glass plates. Shibuichi et al.[17] made super-repellent surfaces (for water and oil) using fractal structures of PFDTS-treated anodically oxidized aluminum surfaces. Superhydrophobicity of silanized microstructured silicon substrates was described by Barbieri et al.,[18] while Li et al.[19] achieved superhydrophobicity of hierarchical structures consisting of monolayer polystyrene colloidal crystals decorated with single- and multiwalled carbon nanotubes. Klein et al.[20] used PFDTS on silica-coated alumina samples to fabricate superhydrophobic surfaces, and very recently, PFDTS was applied to multilength scale structures based on silica particles for nonwettable cotton textile applications.[12]

In all these studies, the only role of the fluoroalkylsilane polymer coating was to reduce the surface energy by creating a hydrophobic layer on smooth or micro/nanostructured substrates. However, as discussed above it was recognized long ago that surface roughness has an even more pronounced effect on the hydrophobicity.[21] In the present work, we show that, under specific experimental conditions, the adsorption of PFDTS on silica sphere arrays can lead to the self-assembled formation of nanostructures. Therewith, the role of the fluoroalkylsilane polymer is twofold: it (i) simultaneously reduces the surface energy and (ii) leads to an increase of the surface roughness. As far as we are aware, this is the first time that such a double role for PFDTS is reported. We investigate the effect of PFDTS treatment on smooth oxide-coated silicon substrates, as well as on monolayer and multilayer arrays of silica microspheres with varying diameters in the nanometer regime. Additionally, we study the role of residual water during PFDTS adsorption and discuss the formation mechanism of the fluoroalkylsilane nanostructures. The wetting behavior of the surfaces with PFDTS-induced multiscaled roughness is analyzed and discussed in relation to the fabrication conditions.

Experimental Details

Materials. Silica microspheres of 830, 440, and 140 nm diameter (as determined by SEM analysis) were purchased from Bangs Laboratories Inc. in aqueous suspension with solid contents of 10 wt %, 9.9 wt %, and 9.8 wt %, respectively. 1*H*,1*H*,2*H*,2*H*-Perfluorodecyltrichlorosilane (PFDTS, $CF_3(CF_2)_7(CH_2)_2SiCl_3$, 97.0%) was obtained from ABCR GmbH&Co KG-Germany and was used as received without any further purification. All other chemicals (ethylene glycol 99.5%, sulfuric acid 97%, hydrogen peroxide 30%, toluene 99.9%, and ethanol) were of analytical grade from Merck. Water with a resistivity of 18.2 MΩ. cm, purified in a Milli-Q system, was used for the preparation of aqueous solutions, for sample preparation, and for contact angle measurement.

Sample Preparation. Substrates (1×1 cm^2 pieces) were cleaved from polished silicon wafers, covered with a 2.2 nm native oxide layer. After ultrasonic cleaning in methanol for 15 min, samples were immersed in piranha solution (mixture of sulfuric acid and hydrogen peroxide H_2SO_4/H_2O_2 = 3:1 (v/v)) for 30 min and rinsed thoroughly with purified water and dried in a N_2 flow.

Self-Assembly of Silica Microspheres. Deposition of silica microsphere monolayers was achieved using the solvent evaporation method.[22] Briefly, a drop of silica microsphere suspension was deposited on a slightly tilted silicon substrate, and the whole setup was placed in a controlled humidity environment at room temperature. As the solvent evaporated, the microspheres self-assembled into hexagonally close packed (hcp) arrays on the silicon substrate under the action of capillary forces.[23]

Multilayers of silica microspheres were fabricated by using spin coating[24] (WS-400B-6NNP-lite Spin Coater, Laurell, USA). Prior to depositing the silica spheres, the aqueous suspensions were centrifuged (Z36HK centrifuge, Hermle, Germany) at 6000 rpm for 5 min. After three cycles, the silica spheres were redispersed in a mixture of ethanol and ethylene glycol in ratio 100:1 (v/v) by ultrasonication in ice, keeping the solid contents constant; ethylene glycol was added to lower the evaporation rate of the solvents. For spin coating, all samples were prepared at a rotation speed of 3000 rpm for 60 min followed by 3500 rpm for 20 s, using a 25 μL droplet of the suspension. Four coatings were applied on each sample to obtain multilayers of sufficient thickness.

Surface Treatment with PFDTS. To modify the surface chemistry, freshly prepared samples were immersed into a 1% (v/v) solution of PFDTS in toluene for 30 min in air at room temperature (kept constant at 20 °C) with 14% relative humidity, followed by rinsing with pure toluene and drying in a N_2 flow. Considering the solubility of water in toluene,[25] we estimate the water content in the actual solvent to amount to 0.03% (v/v). For PFDTS treatment in the N_2-filled glovebox, a 1% (v/v) solution of PFDTS was prepared with anhydrous toluene, and samples were immersed for 30 min and subsequently rinsed with water-free toluene. Prior to treatment, all samples were placed in the glovebox for 24 h.

Surface Analysis and Measurements. The surface morphology of the structured samples was determined by scanning electron microscopy (SEM-HR-LEO 1550 FEF) or scanning helium ion microscope (HIM-ORION-USA). Contact angle measurements were performed using the sessile drop method on a Dataphysics OCA15+ goniometer under ambient conditions at room temperature. Typically, 4 μL or 8 μL water droplets were used for contact angle measurements; values of the contact angle were determined by the average of at least five independent measurements.

Self-Assembled Formation of PFDTS Nanostructures

Prior to studying the formation of PFDTS coatings on silica sphere arrays, we first take a look at PFDTS deposition on

(14) Srinivasan, U.; Houston, M. R.; Howe, R. T.; Maboudian, R. *J. Microelectromech. Syst.* **1998**, *7*, 252.
(15) Breisch, S.; Heij, B.; Lohr, M.; Stelzle, M. *J. Micromech. Microeng.* **2004**, *14*, 497.
(16) Ogawa, K.; Soga, M.; Takada, Y.; Nakayama, I. *Jpn. J. Appl. Phys.* **1993**, *32*, L614.
(17) Shibuichi, S.; Yamamoto, T.; Onda, T.; Tsujii, K. *J. Colloid Interface Sci.* **1998**, *208*, 287.
(18) Barbieri, L.; Wagner, E.; Hoffmann, P. *Langmuir* **2007**, *23*, 1723.
(19) Li, Y.; Huang, X. J.; Heo, S. H.; Li, C. C.; Choi, Y. K.; Cai, W. P.; Cho, S. O. *Langmuir* **2007**, *23*, 2169.
(20) Klein, R. J.; Biesheuvel, P. M.; Yu, B. C.; Meinhart, C. D.; Lange, F. F. *Z. Metallkd.* **2003**, *94*, 377.
(21) (a) Bartell, F. E.; Shepard, J. W. *J. Phys. Chem.* **1953**, *57*, 211. (b) Herminghaus, S. *Europhys. Lett.* **2000**, *52*, 165–170. (c) Dettre, R. H.; Johnson, R. E. In *CA, Wettability*; Advances in Chemistry Series No 43; American Chemical Society: Washington, DC, 1964; p 136.
(22) Micheletto, R.; H. Fukuda, H.; Ohtsu, M. *Langmuir* **1995**, *11*, 3333.
(23) Zhao, Y.; Li, M.; Lu, Q.; Shi, Z. *Langmuir* **2008**, *24*, 12651.
(24) Wang, D.; Möhwald, H. *Adv. Mater.* **2004**, *16*, 244.
(25) (a) Marche, C.; Ferronato, C.; De Hemptinne, J. C.; Jose, J. *J. Chem. Eng. Data* **2006**, *51*, 355. (b) Englin, B. A; Platé, A. F.; Tugolukov, V. M.; Pryanishnikova, M. A. *Khim. Tekhnol. Topl. Masel* **1965**, *10*, 42.

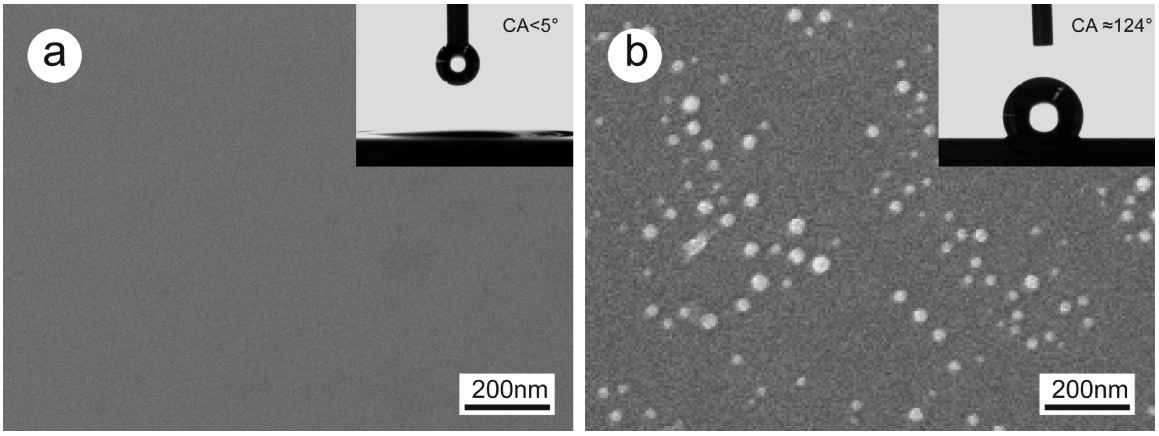

Figure 1. SEM images of oxide-coated silicon substrates before (a) and after (b) PFDTS treatment. The insets depict a water droplet (4 μL) on each of the surfaces.

smooth oxide-covered silicon substrates. In Figure 1a,b, SEM images are shown before and after PFDTS adsorption, respectively. Figure 1b reveals a large density of small bubble-like objects with a spherical cap geometry, which formed during deposition of PFDTS. Similar entities were previously also reported by Bunker et al.[26] and Pellerite et al.[27] during deposition of fluorinated alkyltrichlorosilanes on silicon oxide substrates. Pellerite et al. referred to the spherical objects as "particulates" and showed that their size strongly depends on the immersion time. Bunker et al. studied their so-called "PFDTS spheres" using AFM imaging revealing that the diameter of these "spheres" could be as large as 300 nm. Furthermore, using light scattering experiments they provided convincing evidence that the spheres on the substrate are aggregates similar to those observed in isooctane-based PFDTS solutions and considered to be inverse micelle structures. From Figure 1b, it is obvious that in our case the diameter of the PFDTS-induced entities is much smaller than that of the spheres observed by Bunker et al. The largest diameter found in our experiment amounts to approximately 40 nm, while the smallest ones are well below 10 nm. A possible reason for the smaller average sizes in our experiments could be the considerably shorter immersion time used in the present work.

We suggest that the mechanism for the formation of the aforementioned PFDTS nanostructures is a combination of hydrolysis and condensation reactions both in solution as well as at the substrate surface. The possible reaction steps are schematically represented in Figure 2 and summarized in the following equations:

$$\text{hydrolysis}: \quad R_f - SiCl_3 + 3H_2O \rightarrow R_f - Si(OH)_3 + 3HCl \tag{1}$$

where $R_f = CF_3(CF_2)_7(CH_2)_2$

$$\text{condensation}: \quad n(R_f - Si(OH)_3) \rightarrow [R_f - Si - O - Si - R_f]_n + 3/2nH_2O \tag{2}$$

Details of these hydrolysis and condensation reactions during chlorosilane deposition have been studied extensively by a number of different techniques, including Fourier transform infrared spectroscopy (FTIR), X-ray photoelectron spectroscopy (XPS), energy-dispersive X-ray spectrometry (EDX), light-scattering methods, ^{17}O nuclear magnetic resonance (NMR), and contact angle measurements. The entire process is well-documented in literature. The formation of silane networks (Si−O−Si) was detected by FTIR,[28,29] while the presence of low surface energy elements ($-CF_3$) was confirmed by XPS and verified by contact angle measurements.[12,19,29,30] PFDTS nanostructure (spheres) formation as a result of polymerization on surfaces was studied by AFM,[26,30] while light scattering was used to assess the polymerization process in solution.[26] Our results of SEM and contact angle measurements along with the observation that the PFDTS solution exhibits considerable light scattering (appears milky) when exposed for longer periods to moisturized air is consistent with these literature reports. Therefore, we assume that similar hydrolysis and condensation reactions form the basis for the polymerization, eventually giving rise to the formation of the observed PFDTS nanostructures.

During the hydrolysis reaction shown in Figure 2a, the trichlorosilane endgroups react with water in solution to form hydroxysilane species (silanols), which have a higher affinity for attachment to the surface as compared to chlorosilane. These silanols subsequently will couple to each other and with the substrate primarily via hydrogen bonding,[26] as shown in Figure 2b. Next, covalent bonding[27,29,31−33] during the condensation reaction leads to the formation of cross-linked siloxane networks (Si−O−Si linkages), as represented in Figure 2c. At the surface onto which the PFDTS is deposited, this eventually leads to the formation of a dense and robust film that is highly cross-linked via covalent bonds, both laterally and to the substrate.

Results of experiments in which PFDTS is deposited onto monolayer and multilayer arrays of large silica microspheres (830 nm diameter) are shown in Figure 3. It can clearly be observed from Figure 3a that the PFDTS forms a homogeneous layer on the surface of the silica microspheres within the monolayer. Moreover, close examination of the images in Figure 3a,b reveals the formation of "bridges" between neighboring microspheres,

(26) Bunker, B. C.; Carpick, R. W.; Assink, R. A.; Thomas, M. L.; Hankins, M. G.; Voigt, J. A.; Sipola, D.; de Boer, M. P.; Gulley, G. L. *Langmuir* **2000**, *16*, 7742.
(27) Pellerite, M. J.; Wood, E. J.; Jones, V. W. *J. Phys. Chem. B* **2002**, *106*, 4746.
(28) (a) Arifuzzaman, S; Ozcam, A. E.; Efimenko, K. *Biointerphases* **2009**, *4*, FA33. (b) Vilcnik, A.; Jerman, I.; Vuk, A. S.; Kozelj, M.; Orel, B.; Tomsic, B.; Simoncic, B.; Kovac, J. *Langmuir* **2009**, *25*, 5869. (c) Angst, D. L.; Simmons, G. W. *Langmuir* **1991**, *7*, 2236.
(29) Xu, W.; Liu, H.; Lu, S.; Xi, J.; Wang, Y. *Langmuir* **2008**, *24*, 10895.
(30) Paso, K.; Helberg, R. M. L.; Raaen, S.; Sjoblom, J. *J. Colloid Interface Sci.* **2008**, *325*, 228.
(31) (a) Sagiv, J. *J. Am. Chem. Soc.* **1980**, *102*, 92. (b) Maoz, R.; Sagiv, J. *J. Colloid Interface Sci.* **1984**, *100*, 465.
(32) Fadeev, A. Y.; McCarthy, T. J. *Langmuir* **2000**, *16*, 7268.
(33) Rye, R. R.; Nelson, G. C.; Dugger, M. T. *Langmuir* **1997**, *13*, 2965.

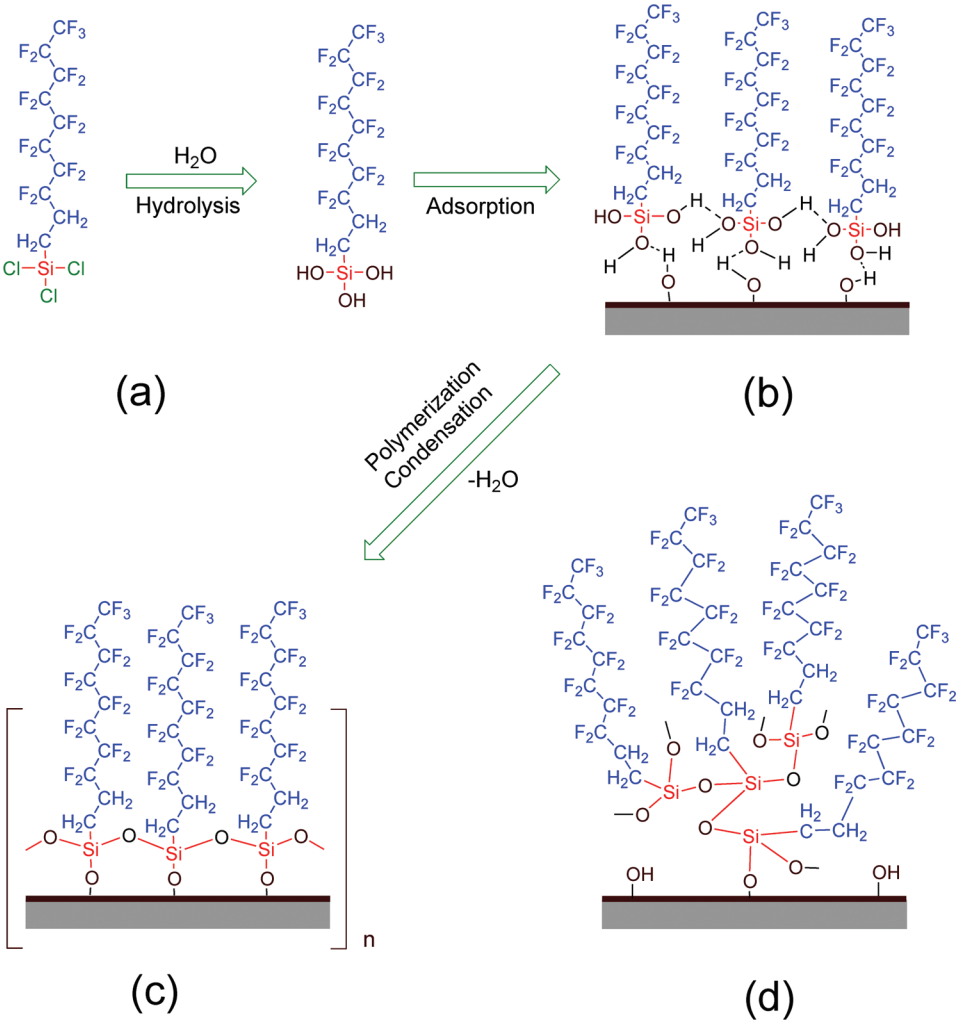

Figure 2. Schematic representation of hydrolysis and condensation reactions occurring during PFDTS self-assembly: (a) Hydrolyzation of trichlorosilane into hydroxysilane; (b) silanol adsorption via hydrogen bonding; (c) formation of siloxane networks via covalent bonding; and (d) vertical polymerization condensation.

as well as between the silica spheres and the substrate. We suggest that due to the polymerization condensation reaction[31,32] (Figure 2c) in solution some additional polymeric material[34] was formed, which subsequently accumulated in between the microspheres, as well as between the spheres and the substrate, developing these bridges which induce strong adhesion among the different components constituting the superstructures.

When the PFDTS deposition was carried out on multilayers of silica microspheres, characteristic extrusions are being formed, as shown in Figure 3c. Since they only form during the coating of the multilayers with PFDTS, the extruding nanostructures are considered to consist of polymerized PFDTS. Careful observation of the PFDTS nanostructures reveals that they appear to consist of an assembly of cubical elements with a typical size of 150 nm. The cross section view in Figure 3d shows that the PFDTS nanostructures are present not only on the uppermost layer, but also within these multilayer arrays. Moreover, it appears that the growth of these nanostructures started from somewhere within the multilayers.

We also investigated the effect of silica sphere size on the formation of PFDTS nanostructures. In Figure 4, the results of PFDTS self-assembly on monolayer and multilayer arrays of smaller silica spheres of 440 nm (Figure 4a−c) and 140 nm (Figure 4d−f) are shown. Again, the PFDTS nanostructures are only observed on multilayer superstructures of silica spheres. However, as is evident from the comparison for different silica sphere diameters in Figures 3 and 4, the size and density of the PFDTS nanostructures appears to increase with decreasing diameter of the silica spheres. In Figure 5, we plot the effective surface coverage of PFDTS nanostructures as determined from large-scale top-view SEM images. A possible explanation for this trend may well be related to the larger surface density of silica spheres. Additionally, for smaller silica spheres the thickness of the multilayer in terms of particle diameters also increases (compare the insets of Figure 5) with the same number of coating cycles (4 for each sample).

The possible hydrolysis and condensation reactions taking place during PFDTS adsorption were already discussed above and schematically presented in Figure 2. It is clear that the condensation reaction not only takes place between hydroxyl groups of surface and silanols, but horizontal condensation occurs also, as shown in Figure 2c, between the silanols themselves, thereby leading to the formation of thick films.[34] Additionally, the hydroxyl groups of the assembling PFDTS molecules can induce vertical polymerization,[32] as shown in Figure 2d to form grafted polysiloxane. We assume that a combined effect of all these reactions leads to the creation of the PFDTS

(34) Zisman, W. A. *Ind. Eng. Chem. Prod. Res. Dev.* **1969**, *8*, 98.

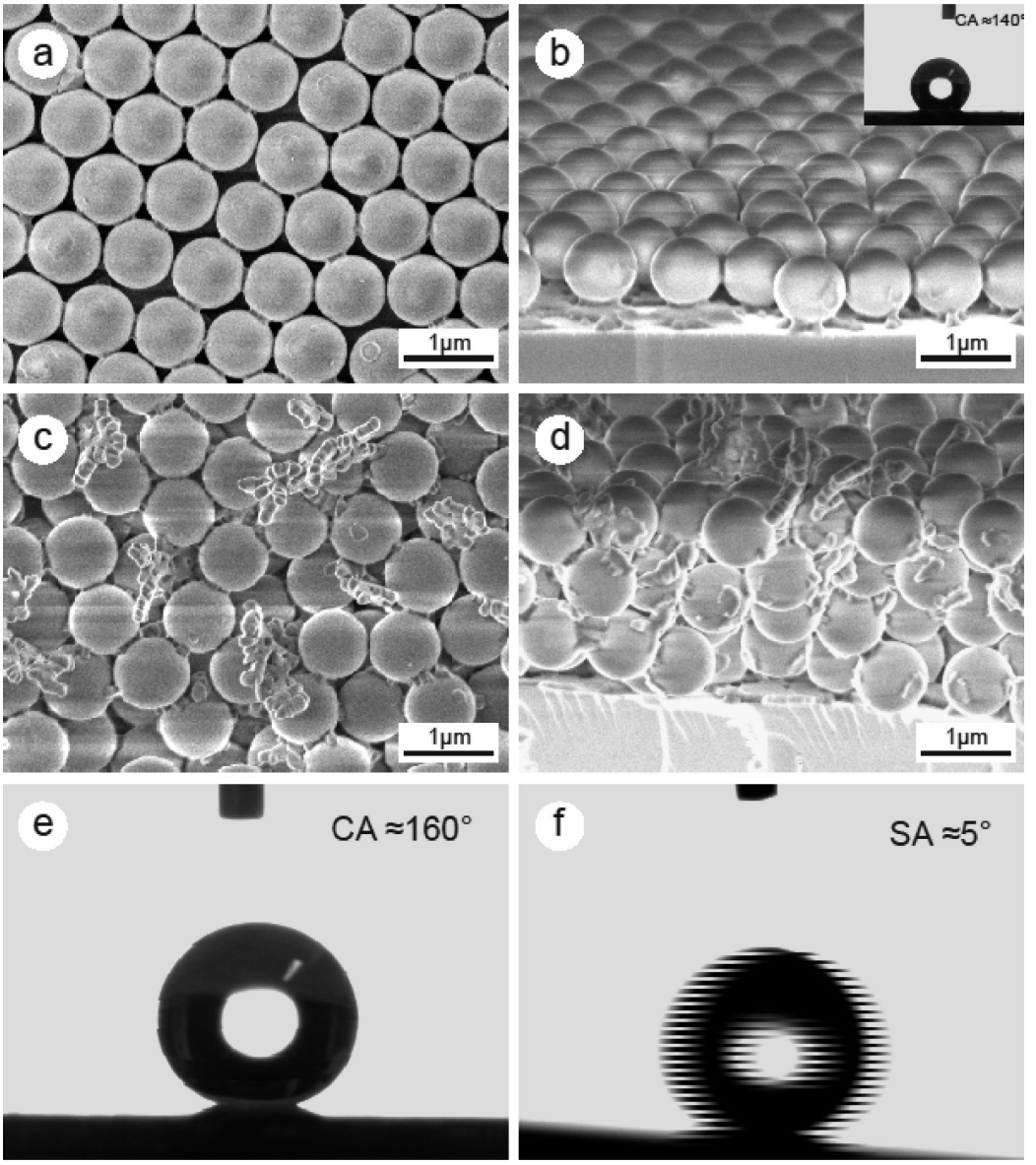

Figure 3. SEM images showing PFDTS self-assembly on 830 nm silica sphere arrays: (a) top view revealing bridge formation between spheres within a monolayer; (b) cross section view of attachment of the spheres with the underlying substrate; the inset depicts a water droplet (4 μL) on a PFDTS-coated silica monolayer; (c) top and (d) cross section views of PFDTS nanostructures self-assembled on silica sphere multilayers. Superhydrobicity of the PFDTS-decorated multilayers as revealed by large static contact angles (e) and a very small sliding angle (f); the water droplet has a volume of 8 μL.

nanostructures.[29] Moreover, the fact that the solution from which the PFDTS is deposited turns cloudy with time confirms the formation of siloxane networks in solution, similar to the "sol−gel" processing of silica.[26,35] Furthermore, the formation of the nanostructures does not appear to be a random process; self-assembly is involved to form the cubic structures (e.g., compare Figure 4b), much like what is observed in micelles in oil−water−surfactant systems, where different hierarchical phases (e.g., lamellar hexagonal and cubic) are typically observed.[36]

In all the aforementioned processes of PFDTS polymerization,[37] water is a key factor. The experiments for which the results are summarized in Figures 3, 4, and 5 were all performed under ambient conditions. This implies that the solvent (toluene) used for the PFDTS solutions contains a finite amount of water. McGovern and co-workers[37] conducted a systematic and quantitative study of the importance of water in the solvent during trichlorosilane deposition. For toluene, they found from XPS measurements that water contents exceeding 0.3 mg/100 mL lead to polymerization in the solution. Considerably lower values (typically 0.15 mg/100 mL) give rise to close-packed chlorosilane monolayers. Additionally, they concluded that even anhydrous toluene at 20 °C in a drybox is able to extract very small but sufficient amounts of water from the substrate for polymerization to take place.

The evaporation rate of toluene is considerably higher than that of water, leading to increasing concentrations of water during the PFDTS treatment procedure. We assume that, during this evaporation, there may be an uneven distribution of water[38]

(35) Prabakar, S.; Assink, R. A.; Raman, N. K.; Myers, S. A.; Brinker, C. J. *J. Non-Cryst. Solids* **1996**, *202*, 53.
(36) Tiddy, G. *J. T. Phys. Rep.* **1980**, *57*, 1.
(37) McGovern, M. E.; Kallury, M. R.; Thompson, M. *Langmuir* **1994**, *10*, 3607.
(38) Britt, D. W.; Hlady, V. *J. Colloid Interface Sci.* **1996**, *178*, 775.

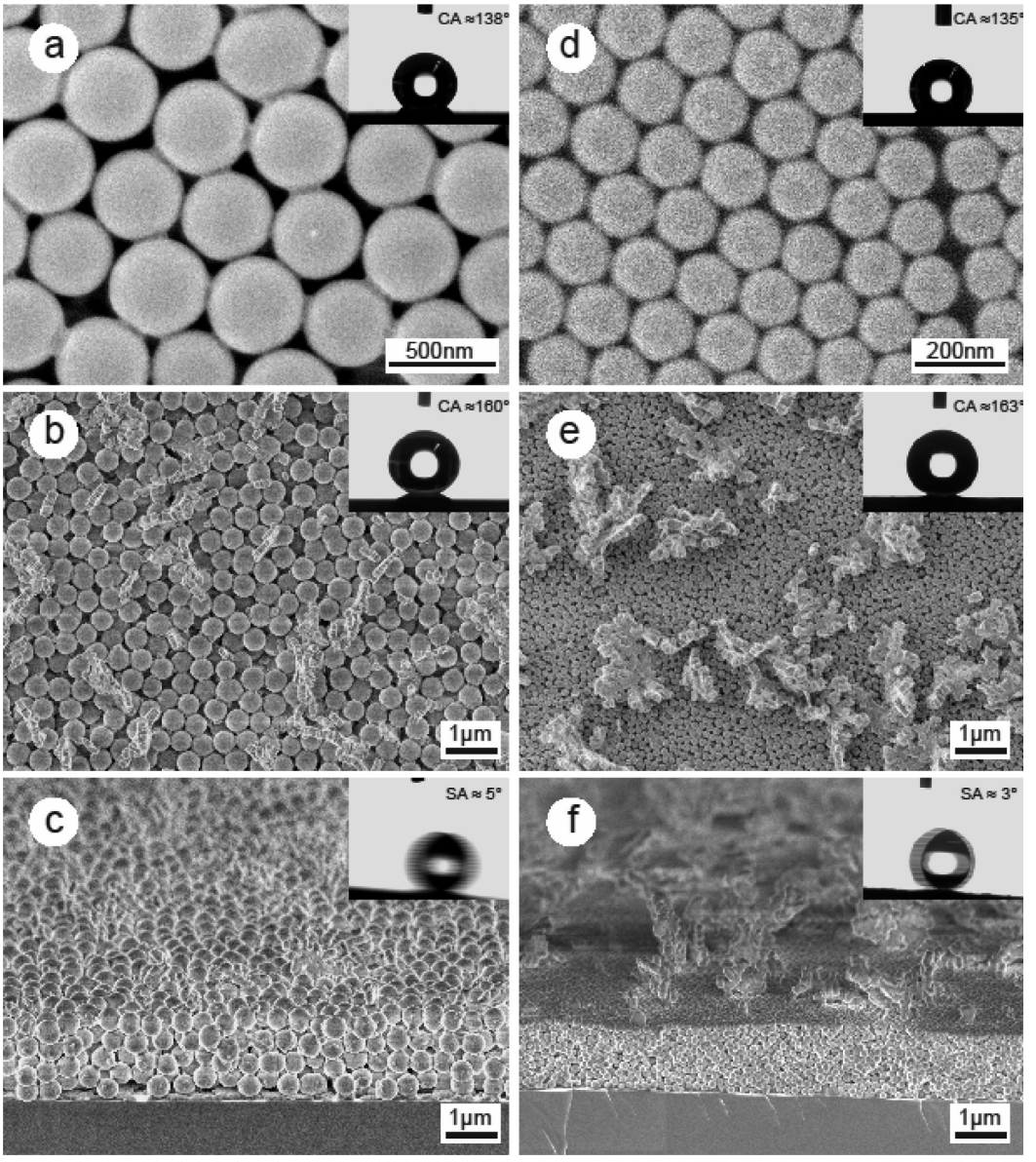

Figure 4. SEM images showing PFDTS self-assembly on 440 nm (left; a−c) and 140 nm (right; d−f) silica sphere arrays: (a,d) Top view of monolayer arrays, showing bridging by the PFDTS coating; insets show a water droplet (4 μL) on each surface. (b,e) Top and (c,f) cross section views of PFDTS nanostructures self-assembled on multilayered silica sphere arrays; insets show the superhydrophobic nature (8 μL water droplet), exhibited by large static contact angles (b,e) and very small sliding angles (c,f).

within the multilayered superstructures, which develops into "water pockets". The pockets of relatively high water contents then act as nucleation sites for the polymerization of the PFDTS to form the characteristic nanostructures. Owing to the limited thickness and relatively open structure of the monolayer arrays, these water pockets are absent or perhaps of much lower concentration, thereby only giving rise to the aforementioned bridge formation; nucleation and growth of PFDTS nanostructures does not occur. Moreover, the larger silica sphere density and thicker multilayers for smaller silica diameters (Figure 5) will give rise to a larger density of relatively more confined water pockets. This in turn explains the higher-density PFDTS nanostructures observed for smaller silica spheres, while the more confined nature of the water gives rise to larger entities extruding from the arrays.

To verify the effect of water on the self-assembly of the PFDTS nanostructures, as discussed above, we performed a control experiment under controlled atmosphere conditions. The experiment on multilayer arrays of 440 nm silica spheres was repeated in a N_2-purged, i.e., water-free glovebox, while PFDTS solutions were prepared using anhydrous toluene to minimize the presence of water during PFDTS treatment. Prior to deposition, samples were placed in the glovebox for at least 24 h. In Figure 6, the result of this experiment is shown and can be compared to the ambient-condition samples as shown in Figure 4b. In the absence of water, the PFDTS nanostructures are not formed at all, thereby providing direct evidence that water is indeed a key factor in the formation of these entities.[31,39]

(Super)hydrophobicity of PFDTS Nanodecorated Substrates

The wetting behavior in terms of the static contact angle (CA) and the sliding angle (SA) of the (nano)structured surfaces

(39) Untereker, D. F.; Lennox, J. C.; Wier, L. M.; Moses, P. R.; Murray, R. W. *J. Electroanal. Chem.* **1977**, *81*, 309.

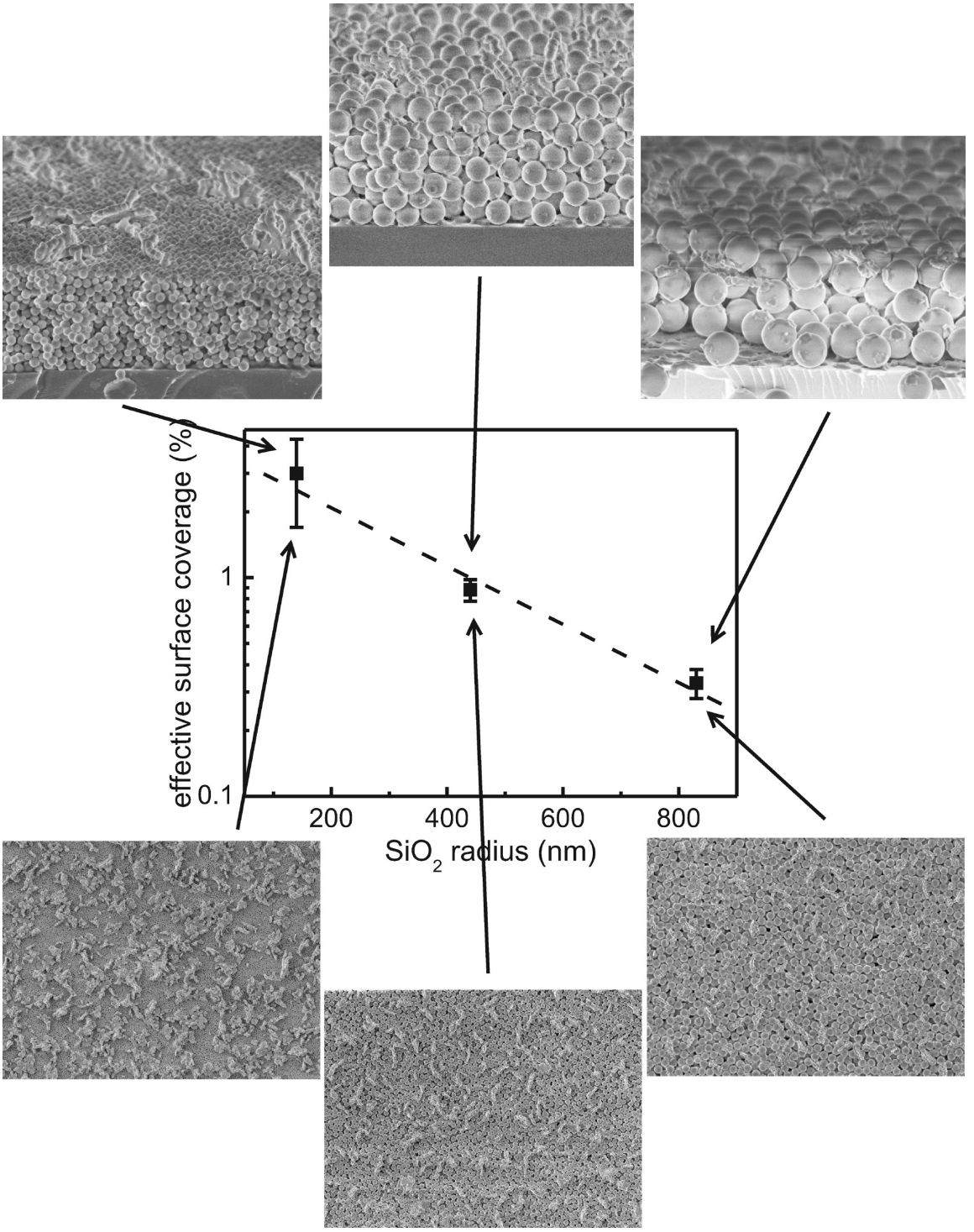

Figure 5. Effective surface coverage of PFDTS nanostructures as a function of the radius of the silica spheres comprising the multilayered arrays. The spatial extent, density, and height of the nanostructures varies with silica sphere size.

described in the previous section are summarized in Table 1; for comparison, calculated values for silica sphere array samples are also included. Here, we analyze and discuss the wettability of these surfaces in relation to their morphology. In general, the wetting behavior of structured surfaces can be explained by the Wenzel[40] and Cassie−Baxter[41] models, which are well-known and frequently used to describe the effects of surface roughness on wettability.

In the Wenzel model, the roughness of a chemically homogeneous surface acts as an amplifier for the wetting or dewetting properties. The important parameter in this model is the roughness factor r, defined as the ratio between the actual and projected surface areas. Wenzel's equation provides a relation among the roughness factor r, the CA θ on a smooth surface, and the CA θ_w on the rough surface

$$\cos \theta_w = r \cos \theta \quad (3)$$

In Wenzel's regime, the liquid is assumed to penetrate into the cavities of the surface structure. However, as the roughness factor

(40) Wenzel, R. N. *Ind. Eng. Chem.* **1936**, *28*, 988.
(41) Cassie, A.; Baxter, S. *Trans. Faraday Soc.* **1944**, *40*, 546.

Table 1. Summary of Wettability Measurements on the Various Substrates, and Comparison to Calculated Values, as Described in This Work[a]

	before PFDTS treatment			PFDTS treatment in open air			PFDTS treatment in N_2-filled glovebox		
silicon oxide substrate	CA < 5°			CA = 124°; SA > 80°			CA = 115°; SA > 80°		
	monolayers			multilayers					
silica spheres size	CA (°) exp.	CA (°) the.[b]	SA (°)	CA (°) exp.	CA (°) the.[c]	SA (°)			
830 nm	140	139	50	160	176	5			
440 nm	138	137	54	160	174	5			
140 nm	135	134	60	163	169	3			
440 nm, (PFDTS treatment in N_2-filled glovebox)	136	134	55	144	143	50			

[a] Contact angle (CA) and sliding angle (SA) values (error ±1°) are determined from the average of at least five independent measurements. [b] Calculated using eq 10, using r_l = 1.2, 1.1, and 1.0 for 830 nm, 440 nm, and 140 nm sphere arrays, respectively. [c] Calculated using eq 5, as described in the text.

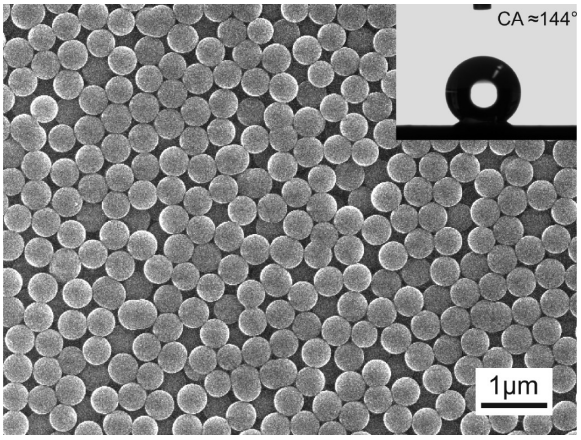

Figure 6. HIM image of 440 nm silica multilayered array after PFDTS self-assembly in a controlled environment (dry nitrogen glovebox). The inset depicts an 8 μL water droplet deposited on the substrate.

crosses a critical value,[42] liquid cannot further penetrate due to the entrapment of air pockets[18] between cavities of surface structures. This regime in which the liquid only partially wets the surface is referred to as the Cassie−Baxter regime. The air acts as second material (with an effective contact angle $\theta = 180°$) giving rise to a heterogeneous liquid interface. The wettability of such surfaces can be modeled by Cassie and Baxter equation

$$\cos\theta_{CB} = f_1 \cos\theta - f_2 \quad (4)$$

where f_1 and $f_2 = 1 - f_1$ are the surface area fractions of solid−liquid and air−liquid interfaces, respectively; θ_{CB} and θ represent the CAs for water on rough and smooth surfaces of the same material, respectively. Most often, the wetted fraction f_1 is not smooth, but also exhibits roughness, introduced by a roughness factor r_f. In this case, the combined effects of chemical composition by the presence of air at the interface and roughness on the wettability is given by[43]

$$\cos\theta_{CBr} = r_f f_1 \cos\theta - (1 - f_1) \quad (5)$$

Furthermore, the sliding angle SA can be used to describe the dynamic wetting behavior and is defined as the surface inclination angle α at which a (water) droplet starts rolling on the surface[44]

$$mg\cdot\sin\alpha/w = \gamma_{lv}\Delta\theta \quad (6)$$

where m is mass of the droplet, g is the gravitational constant, γ_{lv} is the free energy per unit area of liquid−air interface, $\Delta\theta$ represents the CA hysteresis, i.e., the difference between advancing and receding CAs, and w is the length of three-phase (solid−liquid−air) contact line (triple line). Since m, g, and γ_{lv} are constant for a given droplet, the SA α only depends on w and $\Delta\theta$.

The bare silicon surface, cleaned with the piranha solution, exhibits very small contact angles CA < 5° (inset of Figure 1a). The high wettability is a result of the high surface energy of the oxide-coated substrate due to hydroxyl terminating layer. The wettability of the surface dramatically changes (CA ≈ 124°, inset in Figure 1b) after PFDTS treatment owing to the fact that fluorine is well-known to reduce the surface energy due to its smaller atomic radius and high electronegativity.[45,46] The water contact angle CA ≈ 124° is higher than that of a flat surface after PFDTS treatment in N_2-filled glovebox (CA ≈ 115°) and the maximum CA value on a hexagonally close-packed SAM of $-CF_3$ groups (CA ≈ 120°).[46] The reason for this is the roughness induced by the small spherical objects (see Figure 1b)[26] and can be accounted for by Wenzel's law. On the basis of several SEM images such as that in Figure 1b and considering hemispherical features, we estimate the roughness factor to amount to $r = 1.3$. Inserting this into eq 3 together with the CA value $\theta = 115°$ for flat surfaces, we obtain a theoretical value $\theta_w = 124°$, in good agreement with the experimental value. Moreover, large values of the SA on these surfaces indicated that PFDTS-coated silicon oxide substrates are generally sticky hydrophobic surfaces.

In the case of close-packed monolayers of silica spheres (Figures 3a, and 4a,d), after PFDTS deposition the contact angles are even larger (between 135° and 140°; see Table 1) indicating larger values for the roughness factor.

For a more quantitative analysis, we adopt the model as described by Synytska et al.[47] On the basis of the geometry of the close-packed array of spherical caps, they give an expression for the liquid fraction f_1, which is in contact with the spheres, in terms of the liquid penetration depth h and the sphere radius R (see Figure 7):

$$f_1(h) = [2(h/R) - (h/R)^2](\pi/2\sqrt{3}) \quad (7)$$

For the roughness factor, we adopt a slightly different expression than the aforementioned authors, similar to that reported by Xiu et al.:[48]

$$r(h) = 2/(2 - h/R) \quad (8)$$

Please note the difference in definition of h in the works by Xiu et al. and Synytska et al.; we adopt the latter definition (see also the Appendix).

(42) Bico, J.; Tordeux, C.; Quéré, D. *Europhys. Lett.* **2001**, *55*, 214.
(43) (a) Marmur, A. *Langmuir* **2003**, *19*, 8343. (b) Michielsen, S.; Lee, H. J. *Langmuir* **2007**, *23*, 6004.
(44) Furmidge, C. G. L. *J. Colloid Sci.* **1962**, *17*, 309.
(45) Schaub, T. F.; Kellogg, G. J.; Mayes, A. M.; Kulasekere, R.; Ankner, J. F.; Kaiser, H. *Macromolecules* **1996**, *29*, 3982.
(46) Nishino, T.; Meguro, M.; Nakamae, K.; Matsushita, M.; Ueda, Y. *Langmuir* **1999**, *5*, 4321.
(47) Synytska, A.; Ionov, L.; Dutschk, V.; Stamm, M.; Grundke, K. *Langmuir* **2008**, *24*, 11895.
(48) Xiu, Y.; Zhu, L.; Hess, D. W.; Wong, C. P. *Langmuir* **2006**, *22*, 9676.

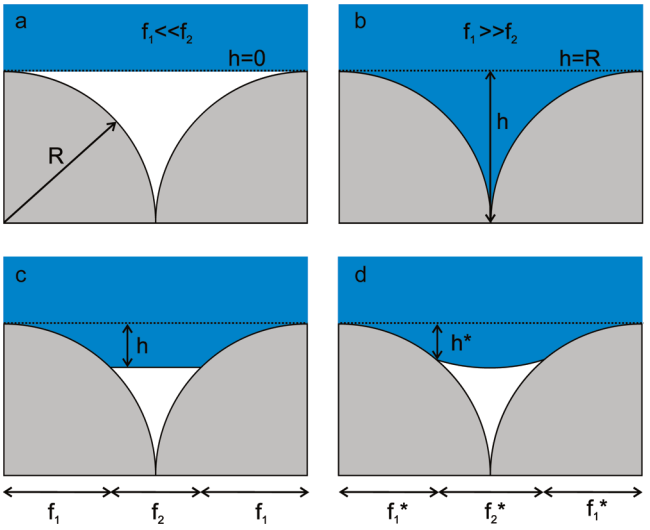

Figure 7. Schematic representation of the different ways the liquid is in contact with the layer of solid hemispheres: (a) flat liquid interface; the liquid only touches the top of the spheres giving maximum values of f_2; (b) complete wetting; the liquid is in contact with the top half of the spheres and fills the whole grooves making the values of f_2 minimum; (c) partial wetting; perfect horizontal liquid−vapor interface with uniform h; (d) curved liquid−vapor interface resulting in smaller values of h^* and larger values of f_2^*.

Inserting eqs 7 and 8 into eq 5 provides an expression for the effective contact angle for a partially wetting surface in terms of the penetration depth of the liquid. Obviously, both expressions show that the absolute sphere dimension does not affect the CA values; this is in agreement with literature reports.[49] Moreover, for the case of a flat liquid interface, which only touches the top of the spheres (Figure 7a), $h = 0$ and accordingly $f_1(0) = 0$ and $r(0) = 1$. For complete wetting of the top halves of the spheres (Figure 7b), we find $f_1(R) = \pi/2\sqrt{3} = 0.907$ and $r(R) = 2$.

For the penetration depth h, Synytska et al.[47] give an expression in terms of the CA θ on a flat surface

$$h = R(1+\cos\theta) \tag{9}$$

which is based on the assumption of a perfectly horizontal liquid−vapor interface between the spheres (Figure 7c; see also the Appendix). If we combine all the aforementioned expressions and insert the value of the CA ($\theta \approx 115°$) on flat silicon oxide after PFDTS treatment in a N_2-filled glovebox, a value of $\theta_{CBr} \approx 134.2°$ is obtained (from eq 5). This is only slightly smaller than the experimentally observed values (135−140°) as summarized in Table 1.

The discrepancy between the modeled value and the actual values can be understood quantitatively by considering that the meniscus (liquid−vapor interface) between the spheres is not perfectly horizontal, but somewhat curved downward owing to the Laplace pressure, as schematically shown in Figure 7d. This gives rise to slightly smaller values of h^* and also results in an additional "roughness factor" r_l (taking into account the curvature) in the last term of eq 5:

$$\cos\theta_{CBr} = r_f f_1 \cos\theta - r_l(1-f_1) \tag{10}$$

The former contribution ($h^* < h$) has little effect on the macroscopic CA, but the latter, i.e., the second term $r_l(1 - f_1)$ in eq 10, gives rise to a noticeable increase of the CA. One can even imagine that, for larger spheres, the curvature becomes more pronounced.[50] Considering roughness factors $r_l = 1.0$, 1.1, and 1.2 for the 140 nm, 440 nm, and 830 nm sphere arrays, calculated values of the macroscopic CA are in good agreement with the experimental values; for comparison, both calculated and experimental values are included in Table 1.

For the case of PFDTS coating of multilayers of silica spheres (440 nm) in a N_2-filled glovebox (Figure 6b), the value of CA is about 144°. Owing to the more random packing of the spheres as observed in the SEM image, the roughness factor will be larger than on the more closely packed monolayers. Consequently, this gives rise to larger contact angles, as is indeed the case (144° compared to 135−140°). Although the CA values approach the superhydrophobicity limit of 150°, the large value of the SA (50°) on this surface shows that superhydrophobicity is still far away.

When PFDTS deposition on the same multilayered arrays of spheres is carried out under ambient conditions, the PFDTS nanostructures described in the previous section are formed. These substrates turn out to be superhydrophobic, characterized by experimental CA values of approximately 160° and small sliding angles SA ≈ 5° (Figures 3 and 4). This increase in hydrophobicity can be explained by considering that the value of f_1 considerably decreases by the introduction of second length scale roughness, similar to what was recently described by Su et al.[6a] The decoration of multilayers of silica spheres with PFDTS nanostructures most likely leads to liquid droplets, which are only in contact with the PFDTS extrusions. Considering that the surface density of PFDTS nanostructures is sufficiently large, the liquid−vapor interface will be approximately flat (i.e., $r = 1$). Inserting the surface coverage values f_1 of Figure 5 into eq 5 with CA $\theta = 115°$ for flat PFDTS surfaces yields calculated CA values ranging from 169° to 176° (see Table 1). These theoretical values are considerably larger than the experimental CAs. Several reasons may account for this discrepancy. For example, we assumed a perfectly flat liquid meniscus on the PFDTS nanostructures, which is obviously too rough an assumption. Additionally, one can imagine that the liquid may also be in contact with the substrate, i.e., the sphere arrays, giving rise to larger f_1 values and thus reduced CA values. Owing to the random nature of the PFDTS nanostructures, this effect is difficult to model.

The large values of $f_2 = (1 - f_1)$ imply that a considerable amount of air is entrapped between the liquid meniscus and the substrate, making the droplet effectively "float" on an air cushion, assisted by the PFDTS nanostructures. This accounts for the very low sliding angles observed for PFDTS nanostructure decorated surfaces. As more asperities are formed as a result of PFDTS self-assembly, the relatively larger air fraction beneath the drop, which cuts the three-phase contact line into discontinuous form and therewith reduces the value of w, gives rise to small values of the SA (eq 6), as low as 3°.

Conclusion

We have investigated the effect of 1*H*,1*H*,2*H*,2*H*-perfluorodecyltrichlorosilane (PFDTS) deposition on bare silicon oxide surface, as well as on monolayer and multilayer arrays of silica spheres having different sizes of 830 nm, 440 nm, and 140 nm. PFDTS deposition was performed both under ambient conditions and in controlled atmosphere (N_2-filled glovebox). The deposition of PFDTS under ambient conditions onto silica sphere arrays led to bridge formation between the spheres on monolayers and generation of special finger-like self-assembled nanostructures on multilayers. It was found that by reducing the size of silica

(49) Tsai, P. S.; Yang, Y. M.; Lee, Y. L. *Langmuir* **2006**, *22*, 5660.

(50) Nakae, H.; Inui, R.; Hirata, Y.; Saito, H. *Acta Mater.* **1998**, *46*, 2313.

spheres the size and number density of formed PFDTS nanostructured protrusion increased. In the absence of water during PFDTS treatment in a N_2-filled glovebox using water-free solvent to minimize the effect of water, PFDTS nanostructures were not formed. It was concluded that self-assembled formation of the PFDTS nanostructures was induced by sufficient amounts of residual water within the multilayers of silica spheres during evaporation of the solvent. The formation mechanism of these structures was discussed considering the hydrolysis and condensation reactions occurring during PFDTS nanostructure self-assembly.

During wettability studies, it was found that hydrophobicity became more pronounced by increasing the roughness of the surface after PFDTS treatment; from flat silicon oxide substrate (CA $\approx$ 124°) to monolayers (CA $\approx$ 140°) and to multilayers (CA $\approx$ 160°). For the monolayer surfaces, we performed a quantitative comparison to a model based on the spherical geometry and found reasonable agreement with the experimentally observed CA. On the basis of qualitative consideration, we can account for a slight increase of the CA values for larger silica spheres. The self-assembled PFDTS nanostructures give rise to a second length scale roughness on our substrates. Correspondingly, we found that these surfaces exhibit superhydrophobicity as expressed by CA values as large as 163° and negligible sliding angles (SA $\approx$ 3°). We have shown that the wettability of structured surfaces can be tuned by changing roughness (from monolayer to multilayers) and by controlling the conditions during PFDTS deposition, thereby opening a range of wettability-related applications of sticking and nonsticking surfaces in various fields.

Acknowledgment. The authors thank S. Khan (University of Twente) for help with spin coating, M. Iqbal (University of Twente) for use of the N_2-glovebox facility, and W. Ahmed and O. Bliznyuk (University of Twente) for helpful discussions. We gratefully acknowledge the support by MicroNed, a consortium to nurture microsystems technology in The Netherlands. One of the authors (M.A. Raza) acknowledges support from the Higher Education Commission in Pakistan.

Appendix A

Partial Wetting of a Hemispherical Surface. In a number of papers,[47−50] the wetting of a surface consisting of a close-packed array of solid hemispheres is treated. In the various publications, different definitions of relevant quantities are used, while even in some cases, different expressions are given. Here, we give a brief derivation of the equations used in our present work.

In Figure A.1, a schematic representation is shown of a partially wetted surface consisting of close-packed hemispheres. The liquid penetration depth is given by h (see Figure A.1b). Following the work by Synytska et al.,[47] the penetration depth can be directly related to macroscopic contact angle θ the liquid will make on a flat solid surface. When we assume that the liquid meniscus (liquid−air interface) is flat and parallel to the substrate plane, simple goniometric relations (see also Figure A.1b) yield

$$\begin{aligned} & (R-h)/R = \sin(\theta-90) \\ \Rightarrow \quad & 1-h/R = -\cos\theta \end{aligned} \tag{A.1}$$

Rewriting immediately gives the relative penetration depth of the liquid between the solid spheres

$$h/R = 1+\cos\theta \tag{A.2}$$

Limiting cases occur (i) when $\theta = 180°$, i.e., when the liquid only touches the top of the spheres corresponding to $h = 0$, and (ii) when $\theta = 90°$ the liquid completely wets the hemispheres with $h = R$.

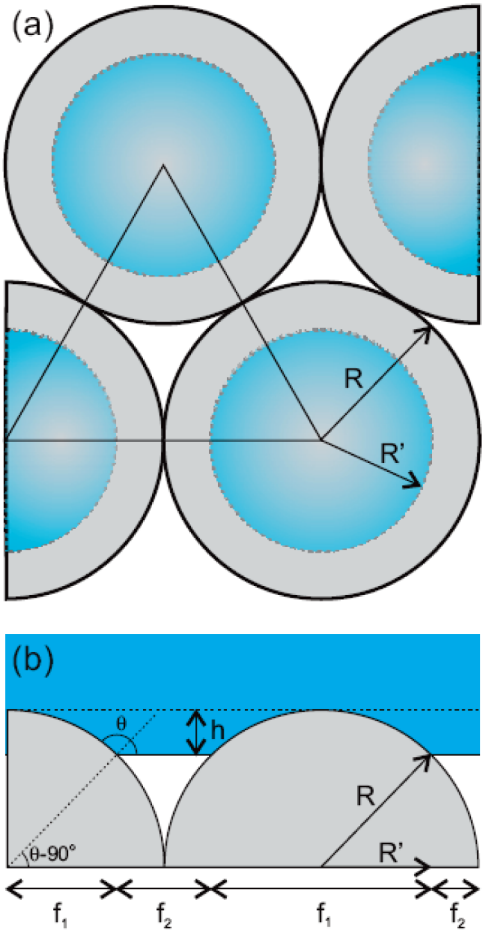

Figure A.1. Schematic top-view (a) and side-view (b) representations of a partially wetted close-packed array of solid hemispheres.

The quantity f_1 represents the projected surface area fraction (see the top-view image in Figure A.1a) of the liquid−solid interface. To derive an expression for f_1, consider the circles with radius R' in the substrate plane. The surface area of the triangular region in Figure A.1a amounts to $R^2\sqrt{3}$, while the wetted area within this triangle is given by $1/2\pi(R')^2$. The ratio of these two quantities defines f_1. To obtain an expression in terms of h/R, we need to determine R'. We know that

$$R^2 = (R')^2 + (R-h)^2 \tag{A.3}$$

Rewriting yields

$$(R')^2 = 2Rh - h^2 \tag{A.4}$$

Inserting this into the aforementioned ratio f_1, we obtain

$$\begin{aligned} & f_1 = 1/2\pi(R')^2/R^2\sqrt{3} \\ \Rightarrow \quad & f_1 = (\pi/2R^2\sqrt{3})[2Rh - h^2] \\ \Rightarrow \quad & f_1 = (\pi/2\sqrt{3})[2(h/R) - (h/R)^2] \end{aligned} \tag{A.5}$$

Again, two limiting cases can be identified: (i) for completely non-wetting conditions, i.e., $h = 0$, we obtain $f_1 = 0$, while (ii) for complete wetting, i.e., $h/R = 1$, we find $f_1 = \pi/2\sqrt{3} = 0.907$; the latter fraction is equal to the relative area of the grey spheres in the top-view image in Figure A.1a.

Finally, we need to determine the roughness factor r for the wetted area fraction f_1. The roughness factor is equal to the ratio

of the actual wetted area, i.e., the spherical cap with radius R and height h, and the projected surface area, i.e., the circle with radius R'. The total surface area of a spherical cap with sphere radius R and height h amounts to $2\pi Rh$. With this and inserting the expression for R', the roughness factor is given by

$$\begin{aligned} & r = 2\pi Rh/\pi(R')^2 \\ \Rightarrow \quad & r = 2Rh/(2Rh - h^2) \\ \Rightarrow \quad & r = 2/(2 - h/R) \end{aligned} \tag{A.6}$$

The same two limiting cases as before can be identified: (i) for $h = 0$, we find $r = 1$ corresponding to a flat horizontal liquid interface, which only touches the top of the spheres, and (ii) for $h = R$, the roughness factor reaches is maximum value $r = 2$.

Note that Synytska et al.[47] use a slightly different expression for the roughness factor r, given by

$$r = 1 + (h/R)^2(\pi/2\sqrt{3}) \tag{A.7}$$

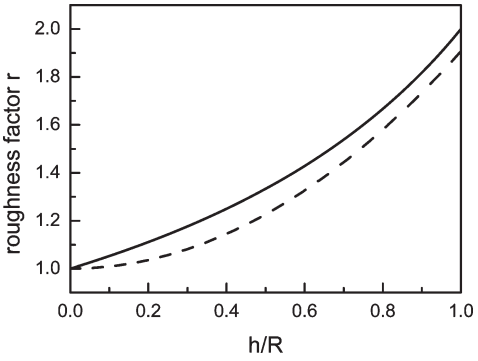

Figure A.2. Comparison of the roughness factors r used in this work (solid line; eq A.6) and as used by Synytska et al. (dashed line; eq A.7).

To compare the expression used in this work (eq A.6) to that of Synytska et al., we plot both roughness factors in Figure A.2 from $h/R = 0$ to $h/R = 1$. Despite quantitative differences, the overall trend is very similar.